A Non-Stationary 3D-GBSM V2V Channel Model for Wideband Massive MIMO Systems

Asad Saleem, Yejun He, *Senior Member, IEEE*, Yan Xu, and Zhi Ning Chen, *Fellow, IEEE*

***Abstract*— This letter presents a non-stationary 3D-GBSM vehicle to vehicle (V2V) channel model in tunnel environment based on massive multiple-input multiple-output (MIMO) antenna arrays. Instead of plane wavefront assumptions used in traditional MIMO systems, the proposed channel model considers spherical wavefront assumption for V2V communications. Firstly, the channel impulse response (CIR) and closed-form expression for probability density function (PDF) of angle-of-departure (AoD) and angle-of-arrival (AoA) in elevation and azimuth planes are derived. Afterwards, the expressions for the spatial cross-correlation function (S-CCF) and doppler power spectrum density (DPSD) due to the non-stationarity of transmitting (NT) and receiving (MR) antenna arrays are derived by considering different time separation, antenna arrays spacing, moving velocity, and K-factor for line of sight (LoS) and non-line of sight (NLoS) propagation paths. The statistical characteristics of the proposed V2V wideband massive MIMO model are validated by measurement, analytical, and simulation results, verifying the effectiveness and adaptability of the proposed model in high-speed train (HST) environment.**

***Index Terms*— Massive MIMO system, cross-correlation coefficients, multipath components, power density function.**

I. Introduction

RECENTLY, the fifth generation (5G) mobile communication system has evolved as a valuable tool to boost the spectrum efficiency and energy in HST environments. Massive MIMO, which utilizes hundreds or more antennas, has grasped an immense attention in recent days due to its potential to provide larger channel capacity [1]. In V2V environments, the majority of the structures, such as buildings, roads, and urban areas have various kinds of vertical surfaces. To assess the non-stationary characteristics of V2V massive MIMO channel, it is essential to take into consideration the channel spatial statistics for various phases and path delays at various locations. In [2], [3], the 3D non-stationary V2V MIMO channel models are proposed based on twin-cluster and Saleh-Valenzuela modeling schemes to address the velocity and transceiver antenna position challenges. In [4], a 3D antenna array model has been proposed for free-space environment, but the impact of Ricean K-factor and doppler shift on V2V channel performance have not been considered for indoor environments. In [5], the 3D-GBSM based on directional antenna arrays is investigated for V2V communications; however the channel statistics based on time delay at different locations are not considered. Based on planar antenna arrays, the work published in [6] is insufficient since it ignores the non-stationary effect on the channel performance. The efficiency of planar antennas is highly reliant on the antenna placement, and the optimal placement itself is dependent on the propagation scenario and geometry of environment, which is regarded as a drawback of planar antennas. In [7], the correlation coefficient based on spherical wavefront is investigated for V2V communications; however the PDF, Ricean K-factor, and DPSD at different moving velocities and at different positions, which are crucial for V2V MIMO systems, are not taken into consideration.

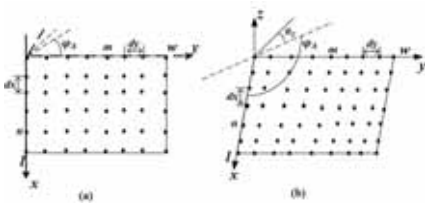

Fig. 1. Geometric antenna array structure by considering (a) plane wavefronts and (b) spherical wavefronts.

In order to fill the aforementioned gaps and high mobility issues in HST environment, this letter presents a non-stationary V2V channel model based on spherical wavefront assumptions to analyze spatial characteristics of massive MIMO antenna arrays in an arched tunnel environment at 3.5 GHz. Analytical expressions for the CIR, PDF of AoD and AoA in elevation and azimuth planes, the DPSD, and cross-correlation functions are derived and validated for different antenna spacing, time separation, and moving velocity of the receiving antenna array for LoS and NLoS propagation paths.

II. Proposed 3D-GBSM V2V System Model

As stated in [6], the far-field of MIMO system is dependent on plane wavefront assumptions as shown in Fig. 1(a), but it is not considered for our proposed V2V channel. This is due to the need of examining the size and dimensions of transmitting (NT) and receiving (MR) antenna arrays. As a result, we consider that the wavefronts transmitted from the scattering elements (S) to the MR antenna arrays are spherical in the proposed V2V system model, as demonstrated in Fig. 1(b). Consequently, the AoA and AoD are not linear anymore throughout the transmission link and need to be determined using geometric relation. The variables d_x, d_y, and d_z in the proposed model represent the transmitting antenna array separating distance along $x-axis$, $y-axis$, and

Manuscript received 6 September 2022; accepted 23 September 2022. Date of publication 26 September 2022; date of current version 9 January 2023. This work was supported in part by the National Natural Science Foundation of China under Grant 62071306, and in part by the Shenzhen Science and Technology Program under Grants JCYJ20200109113601723, JSGG20210802154203011 and JSGG20210420091805014. The associate editor coordinating the review of this letter and approving it for publication was L. Bariah. *(Corresponding author: Yejun He.)*

Asad Saleem and Yejun He are with the Shenzhen Key Laboratory of Antennas and Propagation, College of Electronics and Information Engineering, Shenzhen University, Shenzhen 518060, China (e-mail: asadalvi64@yahoo.com; heyejun@126.com).

Yan Xu is with the School of Opto-Electronic Engineering, Zaozhuang University, Zaozhuang 277160, China (e-mail: xy228826@shu.edu.cn).

Zhi Ning Chen is with the Department of Electrical and Computer Engineering, National University of Singapore, Singapore 119077 (e-mail: eleczn@nus.edu.sg).

Digital Object Identifier 10.1109/LCOMM.2022.3209908

TABLE I
DEFINITIONS OF PARAMETERS

Parameters	Description
d_x, d_y, d_z	Transmitting antenna array separating distance along $x-, y-, z-axes$
d'_x, d'_y, d'_z	Receiving antenna array separating distance along $x-, y-, z-axes$
p, q, r	Half length, Half width, Half height of the arched cross-sectional tunnel
θ_T and φ_T	Elevation and Azimuth angles along transmitting antenna array
θ_R and φ_R	Elevation and Azimuth angles along receiving antenna array
v_R, φ_v	Moving speed, Moving angle of the receiving array
m, n, o	Antenna array elements along $x-, y-, z-axes$
$D, \xi^T_{mno}(t)$	Distance between the transmitted and receiving antenna arrays along $x-axis$, Distance from mno-th transmitting antennas to scatterer (S) at time instant t
w, l, h	Maximum number of antenna array elements along $x-, y-, z-axes$
φ_o, f_{max}, P_u	Initial phase of transmitting signals in azimuth plane, Maximum doppler shift, Mean transmitted power

$z-axis$, respectively. Let's define p, q, and r as half length, half width, and half height of the arched cross-sectional tunnel, i.e., $p \geqslant q \geqslant r$. Here, we consider that receiving array is traveling in the azimuth plane with a speed of v_R and in arbitrary direction φ_v. Table I provides definitions of different parameters used in the proposed model. The CIR of V2V channel is associated to the steering vector components as well as the complex amplitude of the antenna arrays, as given in [8]. Thus, the CIR of massive MIMO system can be stated as

$$h(t) = \sum_{i=1}^{N} a_i(t) \cdot a_{mno}\left(\varphi_A, \theta_E\right) \tag{1}$$

where $a_i(t)$ represents the amplitude in complex form, N represents the total antenna array elements, $a_{mno}\left(\varphi_A, \theta_E\right)$ is a steering vector for mno-th antenna array elements, which may be stated in 3D as m-, n-, and o-th array elements along $x-axis$, $y-axis$, and $z-axis$. φ_A could refer to either the azimuth AoD/AoA (φ_T/φ_R) along the positive $x-axis$, whereas θ_E could refer to either the elevation AoD/AoA (θ_T/θ_R) along the positive y-axis. The steering vector can be written as

$$a_{mno}\left(\varphi_A, \theta_E\right) = \text{vec}\left(\begin{bmatrix} 1 \\ e^{im} \\ e^{i2\ m} \\ \cdots \\ e^{i(w-1)m} \end{bmatrix} \left[1, e^{in}, \ldots, e^{i(l-1)n}\right]\right) \tag{2}$$

where vec(.) is the vector operator, $n = k_w d_y \cos(\varphi_A)\cos(\theta_E)$, $m = k_w d_x \cos(\varphi_A)\cos(\theta_E)$, $k_w = 2\pi/\lambda$, and λ is wavelength. When the elevation angle in 3D space is ignored (i.e., $\theta_E = 0$), the steering vector for plane wavefront can be derived, as given in Fig. 1(a).

Most of the subterrestrial and underground communication structures contain multiple reflected surfaces, so the path delay must need to be considered for given environment. As a result, a three-dimensional non-stationary channel model is considered to investigate V2V communications based on massive MIMO antenna array in real tunnel environment, as shown in Fig. 2. For better visualization, we have shown single scatterer along tunnel sidewall in Fig. 2. The randomly distributed scatterers are exiting throughout the tunnels' ceiling and sidewalls, as shown in Fig. 3. The direct (LoS) distance between mno-th transmitting to $m'n'o'$-th receiving antenna arrays at the time (t) can be written as

$$\xi^{LoS}_{mno,m'n'o'}(t) = \Big[\left(v_R t \sin\varphi_v + m' d'_x - m d_x\right)^2 + \left(v_R t \cos\varphi_v + n' d'_y - n d_y\right)^2\Big]^{1/2} \tag{3}$$

For the reflected (NLoS) signals, the distance between the mno-th transmitting antenna and the scatterer (S) from half tunnel lengths (p, q, r) at time instant t is determined as the function of azimuth and elevation angles, as given follows

$$\xi^T_{mno}(t) = \frac{1}{2k_1} \times \left(-k_2 + \sqrt{k_2^2 - 4k_1k_3}\right) \tag{4}$$

where

$$\begin{aligned} k_1 &= q^2r^2\cos^2\theta_T\cos^2\varphi_T \\ &\quad + p^2r^2\cos^2\theta_T\sin^2\varphi_T + p^2q^2\sin^2\theta_T \\ k_2 &= 2q^2r^2nd_y\cos\theta_T\cos\varphi_T - Dq^2r^2\cos\theta_T\cos\varphi_T \\ &\quad + 2p^2r^2md_x\cos\theta_T\sin\varphi_T \\ k_3 &= (D/2 - nd_y)^2 q^2r^2 + p^2r^2(md_x)^2 - p^2q^2r^2 \end{aligned}$$

Moreover, the expression for distance between scatterer (S) and $m'n'o'$-th receiving array is written as follows

$$\begin{aligned} &\xi^R_{m'n'o'}(t) \\ &= \Big[\left(\xi^T_{mno}(t)\right)^2 + \xi^2_{mno,m'n'o'}(t) \\ &\quad -2\xi^T_{mno}(t)\cdot\xi_{mno,m'n'o'}(t)\cos\theta_T\cos\left(\varphi_T - \varphi_0\right)\Big]^{1/2} \end{aligned} \tag{5}$$

where $\varphi_o = \frac{v_R t}{D} \cdot \sin\varphi_v$. The scatterer's cartesian and spherical coordinates from origin point are represented as (X, Y, Z) and (ξ, φ, θ), respectively. In addition, $(\xi^T_{mno}, \varphi_T, \theta_T)$ represents the transmitting array spherical coordinates. Since the angular and radial coordinates both changes in tunnel, it is impossible to simply transfer from (ξ, φ, θ) to $(\xi^T_{mno}, \varphi_T, \theta_T)$. As a result, (ξ, φ, θ) must be transformed into (X, Y, Z) first, then back to $(\xi^T_{mno}, \varphi_T, \theta_T)$. Thus, the joint PDF for cartesian coordinates $f(X, Y, Z)$ is determined as follows:

$$f(X, Y, Z) = f(\xi, \varphi, \theta) \cdot |J(X, Y, Z)| \tag{6}$$

where $|J(X, Y, Z)|$ represents the inverse transformation of Jacobian matrix. The general form of Gaussian density function of scattering element can be expressed as

$$f\left(\xi^T_{mno}(t), \varphi_T, \theta_T\right) = 1/2\pi\sigma^2 \times \exp\left(\frac{-\xi^T_{mno}(t)^2}{2\sigma^2}\right) \tag{7}$$

where $\xi^T_{mno}(t)$ is the distance from mno-th transmitting antennas to scatterer (S) at time instant t, and σ is a standard deviation. The joint PDF for AoD as the function of elevation/azimuth planes, separating distances, and standard deviation can be expressed as

$$\begin{aligned} &f\left(\xi^T_{mno}(t)\ , \varphi_T, \theta_T\right) \\ &= \frac{\left(\xi^T_{mno}(t)\right)^2\cos\theta_T}{2\pi\sigma^2} \times e^{-\frac{1}{2\sigma^2}\times\left(\xi^T_{mno}(t)\sin\theta_T\right)^2} \\ &\quad \times e^{-\frac{1}{2\sigma^2}\times\left(\xi^T_{mno}(t)\cos\theta_T\cos\varphi_T - D/2\right)^2} \times e^{-\frac{1}{2\sigma^2}} \\ &\quad \times \left(\xi^T_{mno}(t)\cos\theta_T\sin\varphi_T\right)^2 \end{aligned} \tag{8}$$

However, when t is changed (i.e., $t \neq 0$), the given channel model turns into non-stationary channel [2]. The marginal PDF for AoD as the function of elevation or azimuth plane can be calculated individually by following the expressions in [9].

III. Characteristics of Proposed V2V System Model

A. Cross-Correlation Function

Let's define q_1 as the transmission link between mno-th transmitting to $m'n'o'$-th receiving arrays. As a result, the multipaths CIR at time t for link q_1 with delay (τ) can be estimated as

$$h_{q_1}(t,\tau) = \sum_{i=1}^{\infty} h_{q_1,i}(t) \cdot \delta\left(\tau - \tau_i(t)\right) \tag{9}$$

Generally, the CIR for the link q_1 contains direct and reflected paths, which may be represented as $h_{q_1,i}(t) = h_{q_1,i}^{LoS}(t) + h_{q_1,i}^{NLoS}(t)$. Also

$$\begin{aligned} &h_{q_1,i}^{LoS}(t) \\ &= \delta(u-1) \times \sqrt{\frac{K}{K+1}} \times e^{j\varphi_o + \frac{j2\pi}{\lambda} \times \xi_{mno,m'n'o'}^{LoS}(t)} \\ &\quad \times e^{j2\pi f_{\max} \cdot \cos\varphi_R \cos\theta_R \cdot t} \end{aligned} \tag{10}$$

$$\begin{aligned} &h_{q_1,i}^{NLoS}(t) \\ &= \sqrt{\frac{P_u}{K+1}} \times \lim_{S\to\infty} \frac{1}{\sqrt{S}} \sum_{i=1}^{S} g_i \\ &\quad \times e^{j\varphi_o + j2\pi f_{\max} t \cos(\varphi_R - \varphi_v)\cos\theta_R + \frac{j2\pi}{\lambda}\left[\xi_{mno}^{T}(t) + \xi_{m'n'o'}^{R}(t)\right]} \end{aligned} \tag{11}$$

where P_u is the mean transmitted power through q_1 between the mno-th transmitting array elements and $m'n'o'$-th receiving array elements, f_{max} denotes the maximum doppler shift, and K represents the Ricean factor [10]. Here, P_u is normalized to 1, so the K can be more effective. In addition, φ_o represents the initial phase of transmitting signals in azimuth plane between [0 - 2π], and the amplitude of the scattering wave towards the receiving array is denoted by g_i; thus$\sum_{i=1}^{S} E g_i^2/S = 1$ when $S \to \infty$. Let q_2 represents the transmission link between the MNO-th transmitting and the $M'N'O'$-th receiving arrays. We suppose that q_1 and q_2 are independent to each other. Here, the mno-th and MNO-th represent the same antenna array structure, but they have been considered to differentiate in two different transmission links (i.e., q_1 and q_2). Thus, the normalized S-CCF at different time intervals for two different NLoS paths (q_1 and q_2) is given by

$$\begin{aligned} &R_{h_{q_1,i}^{NLoS}, h_{q_2,i}^{NLoS}}(t,\tau) \\ &= E\left[\frac{h_{q_1}(t) h_{q_2}^{*}(t-\tau)}{|h_{q_1}(t)| \cdot |h_{q_2}^{*}(t-\tau)|}\right] \\ &= \frac{1}{K+1} \times \lim_{S\to\infty} \frac{1}{S} \sum_{i=1}^{S} E\left[g_i^2\right] \\ &\quad \times e^{j2\pi f_{\max} \cdot \tau \cos(\varphi_R - \varphi_v)\cos\theta_R} \\ &\quad \times e^{\frac{j2\pi}{\lambda} \times \left[\xi_{mno}^{T}(t) - \xi_{MNO}^{T}(t) + \xi_{m'n'o'}^{R}(t) - \xi_{M'N'O'}^{R}(t)\right]} \end{aligned} \tag{12}$$

Clearly, the S-CCF between the two NLoS paths is affected not only by path lengths, but also by the moving direction and velocity.

B. Ricean K-Factor

The Ricean K-factor is considered to evaluate the effectiveness of channel transmission link, such as correlation and capacity of massive MIMO systems. At a fixed SNR ratio, the higher value of K-factor defines the higher spatial correlation of a channel. Thus, the estimation of K-factor is critical for the consideration of V2V channel. The K-factor for complex channel matrix $H(t)$ is calculated as

$$K_{[dB]} = \frac{\varepsilon[|\mathbf{H}(t)|]^2}{2\,\mathrm{var}(|\mathbf{H}(t)|)} \tag{13}$$

where $|.|$ is the matrix determinant operation, ε and var are the mean and variance of $|H(t)|$.

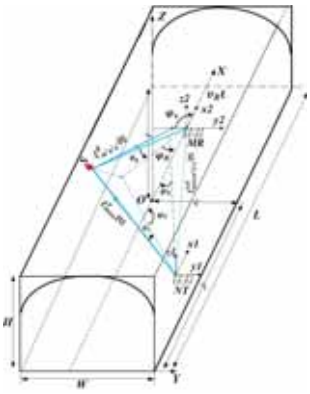

Fig. 2. Proposed 3D-GBSM V2V channel model in tunnel environment.

C. Doppler Power Spectral Density

Let's fix $m = M$, $n = N$, $o = O$, $m' = M'$, $n' = N'$, and $o' = O'$. Afterwards, the spatial auto-correlation function (S-ACF) for LoS and the NLoS components along link q_1 can be estimated as

$$\begin{aligned} &R_{h_{q_1,i}^{LoS}(t,\tau)} \\ &= E\left[\frac{h_{q_1}(t) h_{q_1}^{*}(t-\tau)}{|h_{q_1}(t)| \cdot |h_{q_1}^{*}(t-\tau)|}\right] \\ &= \frac{K}{K+1} \times \lim_{S\to\infty} \frac{1}{S} \sum_{i=1}^{S} E\left[g_i^2\right] \times e^{j2\pi f_{\max} \cdot \cos(\varphi_R)\cos\theta_R \cdot \tau} \\ &\quad \times e^{\frac{j2\pi}{\lambda} \times \xi_{mno,m'n'o'}^{LoS}(t)} \end{aligned} \tag{14}$$

$$\begin{aligned} &R_{h_{q_1,i}^{NLoS}(t,\tau)} \\ &= \frac{1}{K+1} \times \lim_{S\to\infty} \frac{1}{S} \sum_{i=1}^{S} E\left[g_i^2\right] \times e^{j2\pi f_{\max} \cdot \cos(\varphi_R - \varphi_v)\cos\theta_R \cdot \tau} \\ &\quad \times e^{\frac{j2\pi}{\lambda} \times \left[\xi_{mno}^{T}(t) + \xi_{m'n'o'}^{R}(t)\right]} \end{aligned} \tag{15}$$

For the non-stationary channels, the DPSD can be achieved from the auto-correlation function by introducing the Frequency Fourier Transform in time delay (τ) domain, as given below

$$S_{h_{q_1,i}}(t,f) = \int_{-\infty}^{\infty} \left(R_{h_{q_1,i}^{LoS}(t,\tau)} + R_{h_{q_1,i}^{NLoS}(t,\tau)}\right) \times e^{-j2\pi f\tau} d\tau \tag{16}$$

IV. System Performance Analysis

A. Channel Configuration and Measurement Environment

To perform the measurement campaign in V2V environment, we have considered the metro Line 7 in Shanghai between QiHua Rd to University station. The tunnel consists

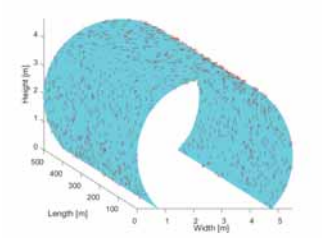

Fig. 3. Randomly distributed scatterers throughout the tunnel ceiling and sidewalls.

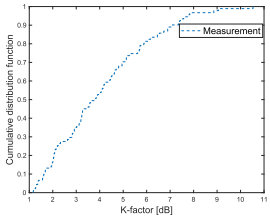

Fig. 4. The cumulative-distribution-function of Ricean K-factor in real tunnel environment.

of arched cross sectional area with 500 m (length) $\times$ 5 m (height) $\times$ 5.56 m (width), and 1500 m radius of curvature (R). The receiving antenna array is moving along $x-axis$ in tunnel environment. The height of transmitting and receiving antenna arrays along $z-axis$ is 1.8 m and 2.7 m, respectively. The separating distance between mno-th transmitting and $m'n'o'$-th receiving antenna arrays along $y-axis$ is 2.48 m, whereas the width of metro track is 1.4 m. The longest distance between mno-th transmitting and $m'n'o'$-th receiving antenna arrays in given wideband measurement campaign is 500 m. Also, 91 different measurement sites are taken into account over this 500 m span. The NT measurement locations are fixed beside the tunnel wall and the MR antenna array is lodged on the trolley moving with 185 km/h along the tunnel central track. The channel configuration and parameters settings are adjusted in accordance with [1].

B. Measurement and Simulated Results Analysis

To begin, we estimate the K-factor by considering CIR of measurement data and following the expression in [10] to ensure that the simulation K-factor is compatible with the measurement data of [1]. Fig. 4 shows the cumulative-distribution-function of Ricean K-factor in measurement campaign, and it can also be observed that the mean value of Ricean K-factor is 4.092 dB. As a result, we chose 4 dB value for K-factor in analytical and simulated results. Moreover, in Fig. 5, we have shown the azimuth angle-of-departure (φ_T), elevation angle-of-departure (θ_T), azimuth angle-of-arrival (φ_R), and elevation angle-of-arrival (θ_R) at separation distance D=50 m between the transceiver antenna arrays. The power angular spread (PAS) is accessed by implementing the Bartlett beamforming method [1]. For radiated field analysis, the Bartlett beamforming method is considered to approximate the PAS out of the actual CIRs' attained from the measurement data, i.e., angle-of-departure (φ_T, θ_T) and angle-of-arrival (φ_R, θ_R). The Bartlett algorithm is anticipated based on the steering vector $a_{mno}(\varphi_A, \theta_E)$ and renowned as the Fourier

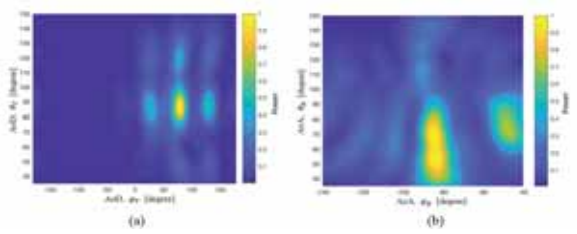

Fig. 5. Power angular spread at 50 m separation distance in measurement campaign for (a) AoD, θ_T and AoD, φ_T, (b) AoA, θ_R and AoA, φ_R.

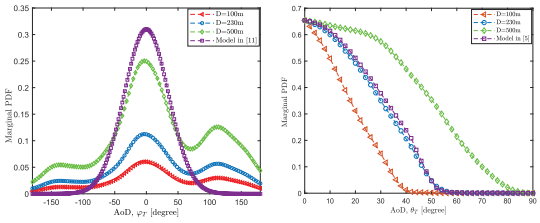

(a) (b)

Fig. 6. Measurement campaign for marginal probability density function (PDF) when $p = 250$ m, $q = 2.78$ m, $r = 2.5$ m at different separating distances (D) for (a) AoD, φ_T, (b) AoD, θ_T.

spectrum analyzing process. From Fig. 5, we can observe that the PAS introduces 2 main beams at 85° elevation, and azimuths of 90° and 135° for AoD (see Fig. 5(a)), and at 60° elevation, and azimuth of -85° and -45° for AoA (see Fig. 5(b)), respectively. The reflected waves from the tunnel sidewalls have higher AoA than those from the tunnel ceiling because the tunnel height is lower than the tunnel width. Additionally, the radius of curvature of the tunnel has a greater impact on φ_R than it does on θ_R.

In Fig. 6, the marginal PDF at $D = 100$ m, 230 m, and 500 m is shown for AoD in azimuth and elevation planes. It can be observed that marginal PDF increases with the increase of separating distance D for φ_T and θ_T. According to [9], the initial geometric path length in a multipath channel has a significant impact on the marginal PDF. In [11], it can be noticed that the receiver and transmitter are located at the spheroid's foci. Moreover, when the signals from the transmitter strike at the scatterer point (S), the AoD statistics in φ_T plane are consistent with our proposed V2V model. Based on directional antenna arrays, the model in [5] is used to determine that the AoD exhibits similar changing trends at $0 \leq \theta_T \leq 90^\circ$ in vertical direction, as shown in Fig. 6 (b). In Fig. 6, each marginal PDF curve for AoD in φ_T and θ_T plane is symmetric due to the symmetry of a geometric V2V model, which is consistent with [11]. Consequently, the proposed 3D-GBSM channel model can be adopted to describe the actual HST environment.

Moreover, we analyze the simulation and analytical results to confirm the feasibility of the given channel model. The Monte-Carlo (MC) approach is considered to simulate the S-CCF (LoS + NLoS) and DPSD under various time separations, doppler shifts ($f_R = v_R/\lambda$), and K-factors. As the LoS components of the CIR are deterministic and the NLoS components of the CIR are predicted through random process, so the MC strategy can be utilized to multiply the iterations of

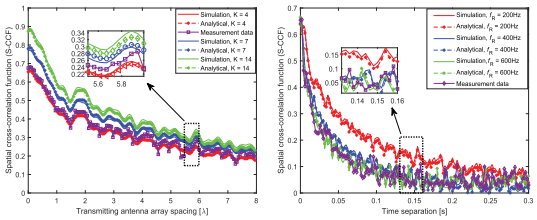

(a) (b)

Fig. 7. Spatial cross-correlation function (S-CCF) of proposed massive MIMO channel at $D = 500$ m, $p = 250$ m, $q = 2.78$ m, $r = 2.5$ m (a) for various K-factor values when $\tau = 1$ ns and $f_R = 600$ Hz, (b) for various time separations (τ) and various doppler shifts (200 Hz, 400 Hz, and 600 Hz) when $K = 4$.

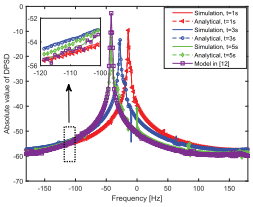

Fig. 8. Simulated and analytical results for doppler power spectrum density (DPSD) at different time intervals.

CIRs' NLoS components. In this letter, the iteration limit for MC approach is set as 3×10^4. For simulation results analysis, we have considered the reflections along the tunnels' ceiling and sidewalls only. The other simulation parameters are set according to measurement campaign in [1]. Fig. 7(a) presents the S-CCF for multiple K-factor values, when $f_R = 600$ Hz, time separation $\tau = 1$ ns, and $D = 500$ m. As shown in Fig. 7(a), the S-CCF decreases as the transmitting array spacing rises, and the S-CCF rises as the K-factor rises. Meanwhile, the measurement results of S-CCF for $K = 4.09$ shows good agreement with the simulation and analytical results of S-CCF, which verifies the validity of the proposed model. The performance of the massive MIMO channel is adversely affected by the LoS components. Fig. 7(b) represents the S-CCF for different time separations (τ) and doppler shifts of 200 Hz (61.7 km/h), 400 Hz (123.4 km/h), and 600 Hz (185.1 km/h) when the $d_x = d_y = d_z = 0.5\lambda$, $K = 4$, and $D = 500$ m. The S-CCF of the measurement results for $f_R = 600$ Hz fits quite well with the the simulation and analytical results, as illustrated in Fig. 7(b). It can be noticed that by increasing temporal separation τ, the S-CCF decreases. When the doppler shift rises, the S-CCF reduces rapidly. As illustrated in [3], the channel characteristics of the V2V MIMO systems are affected by the moving velocity, and this behavior can also be seen in Fig. 7. (b).

In Fig. 8, the DPSD for different time instants $t = 1s$, $3s$, and $5s$ is given when $K = 4$, $f_R = 600$ Hz, $D = 500$ m, $\varphi_v = \pi/2$, $d_x = d_y = d_z = 0.5\lambda$. The DPSD presents different levels at different time instants due to the geometric characteristics of the tunnel when t continuously increases. The DPSD has a noticeable peak, which is due to the high power of dominant LoS components. It can be observed that by increasing t, the DPSD is negatively shifted. Moreover, the doppler power spectrum density (DPSD) is compared with the model in [12], as shown in Fig. 8. Comparison of the simulations and analytical results with the Wu model reveals that the distribution changes are in good agreement, demonstrating the generalizability of the proposed channel model.

V. Conclusion

In this letter, a non-stationary 3D-GBSM V2V channel model based on massive MIMO antenna array is proposed in subway tunnel environment at 3.5 GHz. The spherical wavefronts are considered to characterize the PDF, S-CCF, DPSD, and AoA/AoD in elevation and azimuth planes for V2V communications. It is shown that the non-stationarity, including moving directions φ_v and relative time t significantly affects the V2V channel characteristics. From the simulation, analytical, and measurement results, we conclude that the S-CCF is seriously influenced by K-factor, time separation, antenna array spacing, and moving velocity of receiving antenna array. The proposed V2V channel model results are matching undoubtedly well with former channel models, demonstrating that the given model may be generalized and have practical applications in HST environment.

References

[1] A. Saleem, H. Cui, Y. He, and A. Boag, "Channel propagation characteristics for massive multiple-input/multiple-output systems in a tunnel environment [measurements corner]," *IEEE Antennas Propag. Mag.*, vol. 64, no. 3, pp. 126–142, Jun. 2022.

[2] Q. Zhu, W. Li, Y. Yang, D. Xu, W. Zhong, and X. Chen, "A general 3D nonstationary vehicle-to-vehicle channel model allowing 3D arbitrary trajectory and 3D-shaped antenna array," *Int. J. Antennas Propag.*, vol. 2019, pp. 1–12, Oct. 2019.

[3] Y. Liu, C. X. Wang, J. Huang, J. Sun, and W. Zhang, "Novel 3-D nonstationary mmWave massive MIMO channel models for 5G high-speed train wireless communications," *IEEE Trans. Veh. Technol.*, vol. 68, no. 3, pp. 2077–2086, Aug. 2018.

[4] H. Jiang, Z. Zhang, J. Dang, and L. Wu, "A novel 3-D massive MIMO channel model for vehicle-to-vehicle communication environments," *IEEE Trans. Commun.*, vol. 66, no. 1, pp. 79–90, Jan. 2018.

[5] S. J. Nawaz, N. M. Khan, M. N. Patwary, and M. Moniri, "Effect of directional antenna on the Doppler spectrum in 3-D mobile radio propagation environment," *IEEE Trans. Veh. Technol.*, vol. 60, no. 7, pp. 2895–2903, Jul. 2011.

[6] H. Jiang, Z. Zhang, J. Dang, and L. Wu, "Analysis of geometric multibounced virtual scattering channel model for dense urban street environments," *IEEE Trans. Veh. Technol.*, vol. 66, no. 3, pp. 1903–1912, Mar. 2017.

[7] J. Huang, C.-X. Wang, R. Feng, J. Sun, W. Zhang, and Y. Yang, "Multi-frequency mmWave massive MIMO channel measurements and characterization for 5G wireless communication systems," *IEEE J. Sel. Areas Commun.*, vol. 35, no. 7, pp. 1591–1605, Jul. 2017.

[8] B. Yang, P. Zhang, H. Wang, C.-X. Wang, and X. You, "Broadband extended array response-based subspace multiparameter estimation method for multipolarized wireless channel measurements," *IEEE Trans. Commun.*, vol. 69, no. 5, pp. 3298–3312, May 2021.

[9] J. Zhou, H. Jiang, and H. Kikuchi, "Generalised three-dimensional scattering channel model and its effects on compact multiple-input and multiple-output antenna receiving systems," *IET Commun.*, vol. 9, no. 18, pp. 2177–2187, 2015.

[10] I. B. Mabrouk *et al.*, "Feasibility of a millimeter-wave MIMO system for short-range wireless communications in an underground gold mine," *IEEE Trans. Antennas Propag.*, vol. 61, no. 8, pp. 4296–4304, Apr. 2013.

[11] M. Alsehaili, S. Noghanian, A. R. Sebak, and D. A. Buchanan, "Angle and time of arrival statistics of a three dimensional geometrical scattering channel model for indoor and outdoor propagation environments," *Prog. Electromagn. Res.*, vol. 109, pp. 191–209, 2010.

[12] S. Wu, C. X. Wang, M. M. Alwakeel, and Y. He, "A non-stationary 3-D wideband twin-cluster model for 5G massive MIMO channels," *IEEE J. Sel. Areas Commun.*, vol. 32, no. 6, pp. 1207–1218, Jun. 2014.